FINAL REPORT ESRF ME-1163 (LONG TERM)

"Free volume measurements in metallic glasses and oxide glasses"

[a]A.R. Yavari, [b]A.L. Greer, [c]A. Inoue, [a]W.J. Botta

[a]Institut National Polytechnique de Grenoble (INPG)-CNRS umr 5266, France
[b]Dept Materials Science and Metallurgy, University of Cambridge UK,
[c]Tohoku University, Sendai Japan

This LT project (ME-1163) primarily ID-11 but also ID-15 was part of two broader projects. One was the 6th Framework Programme European RTN Network MRTN-CT-2003-504692 entitled "Ductile BMG Composites" with the participation of the Materials Science group of the ESRF and coordinated by the main proposer A.R. Yavari of Grenoble. The other was the "International Frontier Centre on Advanced Materials IFCAM" coordinated by the co-proposer A.L. Greer of the Univ. of Cambridge and funded by the University of Tohoku of the co-proposer A. Inoue. These projects provided the funding for postdocs (including two years for Dr Magnus Bostrom 2004-2006 at the ESRF) and consumables and provided state-of-the-art off-site support for electron microscopy, atomic force and tunnelling microscopes, calorimetry and other equipment complementary to in-situ diffraction experiments conducted at the ESRF.
In the framework of our previous LT project ME-544, we had used an XRD method to detect and quantitatively measure the amount of *"quenched-in" excess free volume* ΔV_f which is trapped into the glass during fabrication and which anneals out as the glass is heated. Using XRD we also discovered that deformation of glasses results in the generation of *"deformation induced" free volume* which also relaxes out during annealing. In our field of research these results were considered ground-breaking and opened up new possibilities. For example our measurements at the ESRF, of free volume variations during isothermal annealing, were sufficiently precise to allow determination of activation energies controlling the relaxation process (*ESRF Highlights* 2005 pp.35-36). The main purpose of ME-1163 was to continue and extend these studies, both to additional metallic glasses and to oxide glasses and possibly polymer glasses.

Detection and quantitative measurement of quenched-in excess free-volume in metallic and other glasses

Our approach begins with treating the glassy state as a rigid isotropic solid up to T_g. In this approach, the successive broad maxima at wave-vectors Q_{max} corresponding to $I_{max}(Q)$ will elastically move to lower Q values with increasing temperature as a result of thermal expansion and reversibly return to their initial Q_o position upon cooling. An example is given below

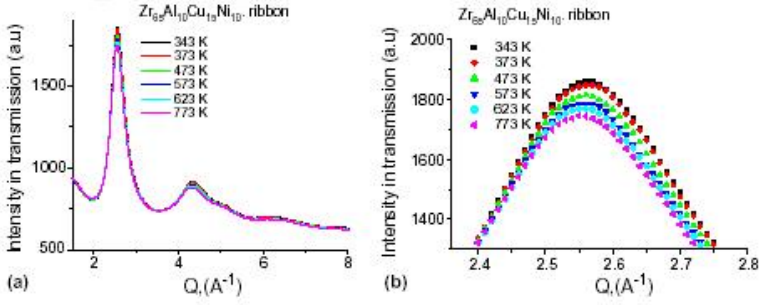

(a) In situ XRD patterns of $Zr_{65}Ni_{10}Cu_{15}Al_{10}$ ribbon subjected to various temperatures during continuous heating and (b) close-up of the maximum of the first amorphous halo in (a).

Any deviations from this reversibility are then discussed in terms of structural relaxation.
In order to search for irreversible phenomena, we use the Ehrenfest relation $Q_{max} = 4\pi\sin\theta_m/\lambda = 1.23(2\pi/a)$ which is obtainable from the Debye formula for the scattering intensity I(Q) and which yields a characteristic atomic dimension and volume V(T) and it follows that:

$$\left\{\frac{Q_{\max}(T^0)}{Q_{\max}(T)}\right\}^3 = \left\{\frac{V(T)}{V(T^0)}\right\} = \left\{1 + \alpha_{th}(T - T^0)\right\} \qquad (1)$$

where α_{th} is the volume coefficient of thermal expansion. From theory, the proportionality constant relating $Q_{max}(T)$ to V(T) in Eq.(1) can change if the structure of the glass (chemical bonding) changes significantly but the constancy of our PDFs across T_g suggests constancy of the proportionality for these BMGs. For each glass studied, we establish plots of eq.(1) during in-situ thermal cycling shown below right. In this example (from ME-544), during initial heating the slope α_{th} is constant with the same value as measured by dilatometry . From T = 425 K, the plot dips until reaching T_g = 590 K. Subsequent heating and cooling show only reversible dilatation. As expected, a slope change occurs at T_g as the glass goes over to the supercooled liquid state.

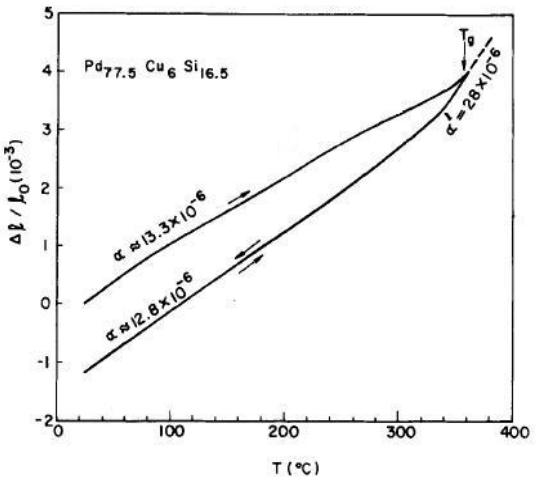

Dilatometric length change of a glassy Pd-based meltspun ribbon showing densification a change of slope at T_g and densification.

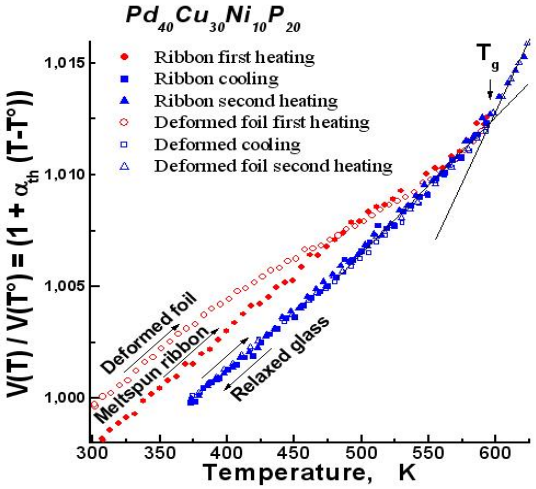

XRD results: Reduced volume per atom of eq.(1) showing relaxation of as-quenched and deformed foils of a Pd-based glass.

The volume difference between the initial as-quenched state and the relaxed state is about 0.2% which corresponds well to densification of other melt-spun metallic glasses as measured by dilatometry and density measurements.

The above type of results (plots of eq.(1)) have now been obtained for a large number of metallic glasses. A few other examples are given below.

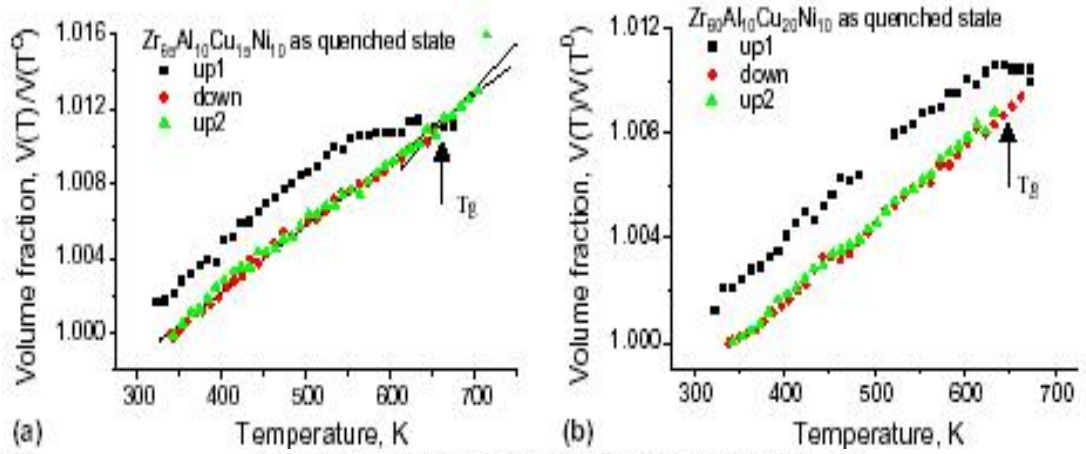

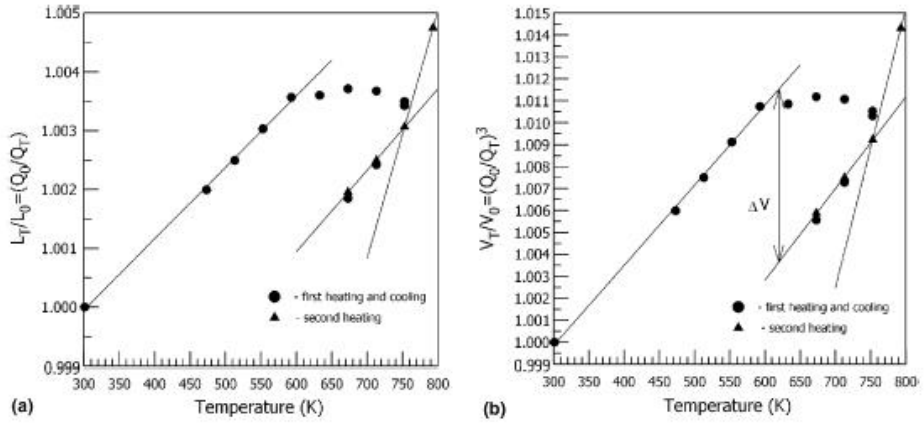

Fig. 3. (a) Q_0/Q and (b) $(Q_0/Q)^3$ values for $Cu_{55}Hf_{25}Ti_{15}Pd_5$ alloy versus temperature. The sample was heated up to 753 K, then cooled down to 673 K and then heated again to 793 K. The preliminary heating up to 753 K was designed to complete the structural relaxation process.

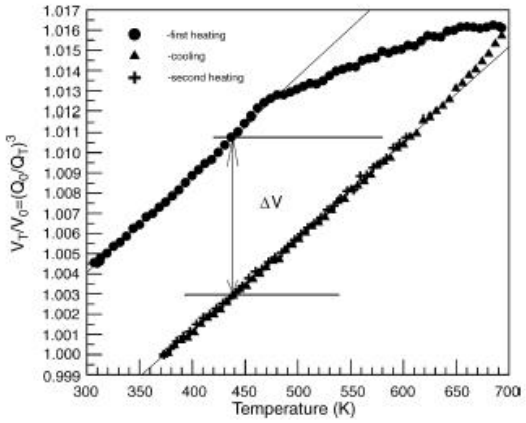

Fig. 3. $(Q_0/Q)^3$ values vs. temperature. The sample was heated up to 693 K, then cooled down to 373 K and then heated again to 603 K. The preliminary heating up to 693 K was designed to complete the structural relaxation process.

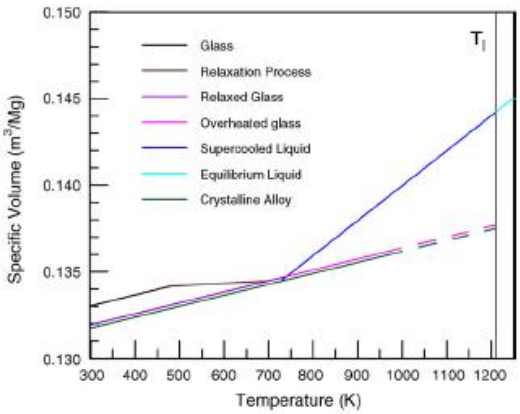

Fig. 4. The specific volume of different phases in the $Cu_{55}Zr_{30}Ti_{10}Pd_5$ alloy as a function of temperature. T_l was measured in ref. [30].

As announced in the work plan, this project also intended to assess the applicability of eq.(1) to oxide glasses in addition to metallic glasses. The following results indicate that this is in fact the case. However, the extent of excess free volume ΔV_f in the oxide glasses is found to be larger than in metallic glasses

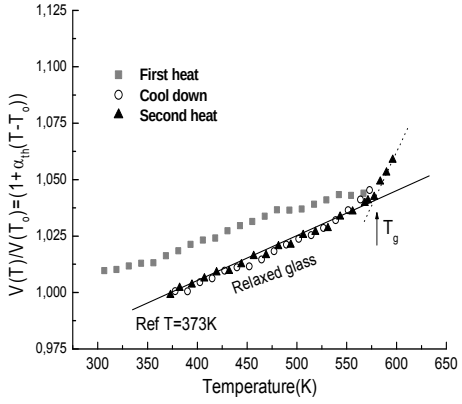

Plot of $\{V(T)/V(T_o)\}$ versus temperature during *in-situ* thermal cycling of air-cooled B_2O_3 glass using eq.(1).

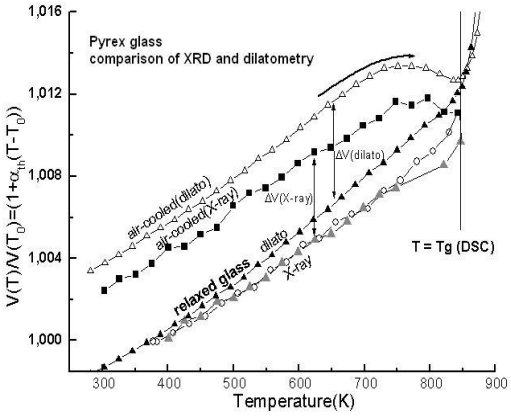

and for Pyrex glass

Detection and quantitative measurement of excess free-volume generated by plastic deformation in metallic glasses

In the work programme, we also aimed at investigating, using eq.(1), the generation of excess free volume by deformation (in addition to ΔV_f due to quenched in free volume).

The next plots are typical of our results obtained using XRD and eq.(1), showing a doubling during deformation (by milling) of ΔV_f to some 0.8% volume.

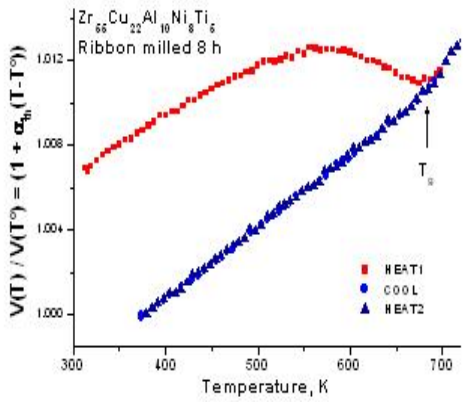

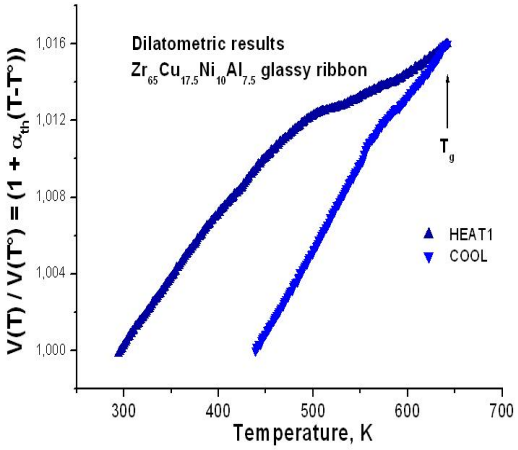

Another example of free-volume generation with deformation and its subsequent annealing out below Tg is given in the next plots.

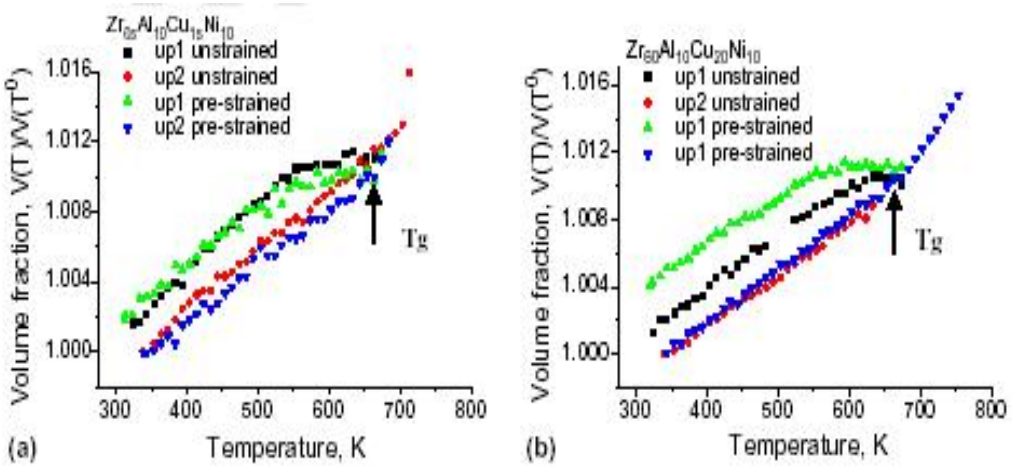

The disappearance of excess free volume ΔV_f has profound practical effects on the mechanical properties of metallic glasses. The next figure and SEM image show how as ΔV_f disappears with heat treatment below Tg, the material becomes harder, showing less deformation and shear banding for the same load as seen in the microhardness indentation tests.

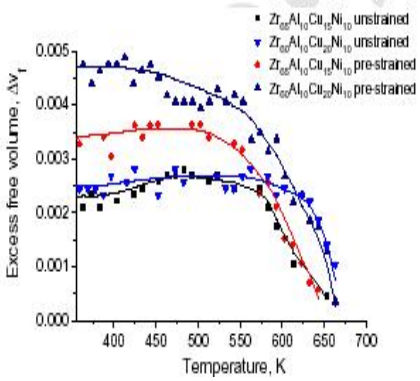

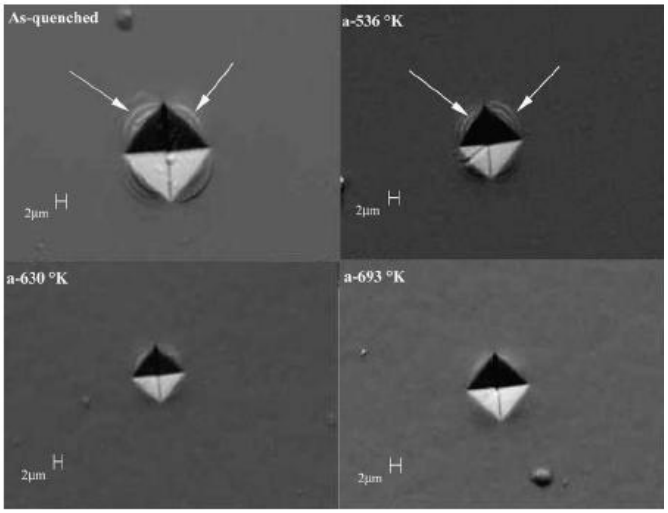

Our XRD experimental method associated with eq.(1) is therefore a versatile method for evaluating the state of relaxation of the specimens with consequences for various properties including mechanical resistance. Nevertheless, although a good one, eq.(1) is still an approximation and volume must in principle be derived from real space and not reciprocal space data. We therefore compared the temperature shift of the maxima of atomic radial pair distribution functions with those of eq.(1).

The reduced radial distribution functions, G(r), were obtained from $Q \cdot I(Q)$ by the usual Fourier transformation with usual corrections and normalisations. The pair distribution functions *g(r)* were then derived using:

$$g(r) = \frac{\rho(r)}{\rho_0} = 1 + \frac{G(r)}{4\pi r \rho_0}$$

with $\rho(r)$ the radial density function and ρ_0 the average atomic number density.

An example (for Cu55Hf25Ti15Pd5 metallic glass) is given in the next plots.

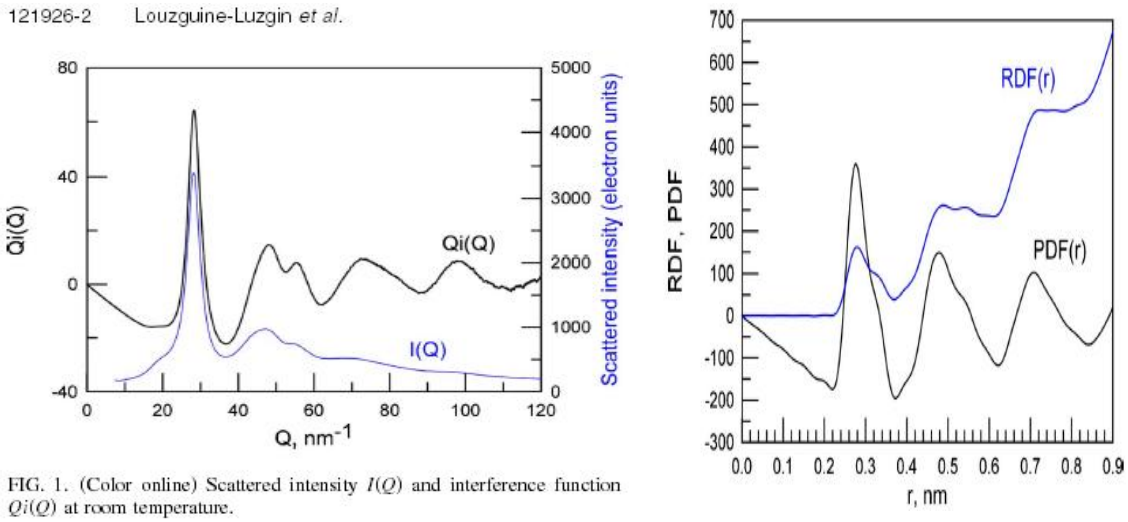

FIG. 1. (Color online) Scattered intensity $I(Q)$ and interference function $Qi(Q)$ at room temperature.

It was found that to within experimental and computational errors, the displacements in reciprocal and real space were proportional but this was only examined for the first maxima.

Effect of crystal nucleation on mechanical properties of metallic glasses

In addition to the study of free-volume in metallic and oxide glasses, we used the Materials Science group beam lines (primarily ID-11 but also ID-15) to heat metallic glasses to the very beginning of crystal nucleation only, such that we obtain a glassy matrix dispersed with extremely fine nanoscale coherent domains. The next screen images of CCD camera data during heating to the onset of crystal nucleation show how fine the changes in diffraction patterns are when we stop heating at nucleation and why the ESRF facilities are indispensable to our collaborative activities (the sharp central peak is from hot-plate glass window, the outer diffuser ring is from the Zr-based metallic glass).

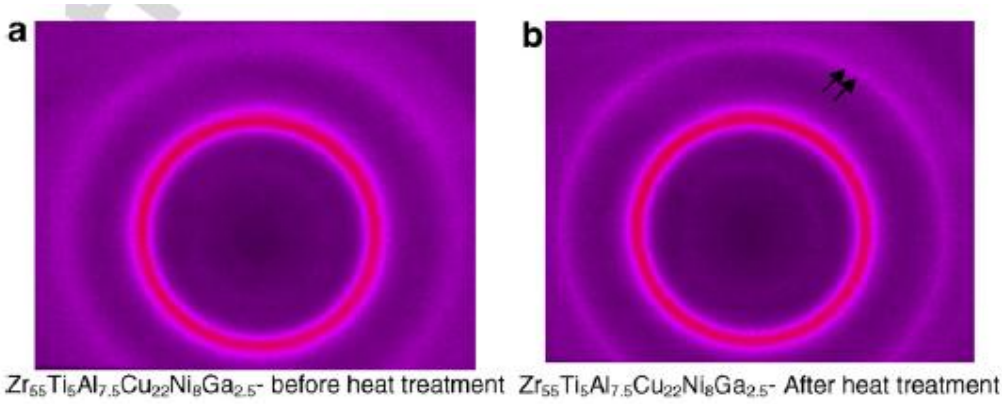

Before and after this delicate heat treatment, the bulk metallic glasses are mechanically tested in uniaxial compression until fracture and some such results are presented in the next stress-strain curves.

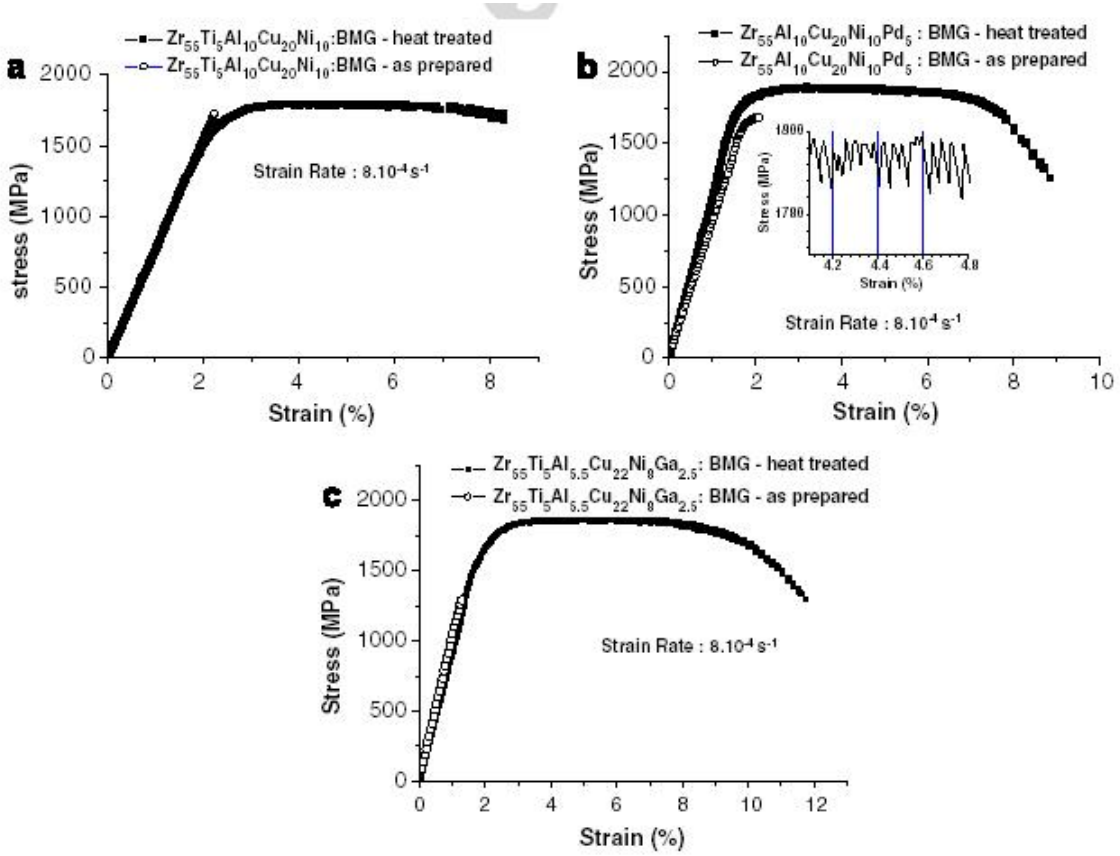

It is seen that in each case, the specimen heated to onset of nanocrystal nucleation undergoes significant plastic deformation to fracture (some to 10%) while the untreated specimen fractures in the elastic range.

SEM examination of the heat-treated specimens after plastic deformation show presence of large numbers of shear bands and shear steps as can be seen in the image on the right.

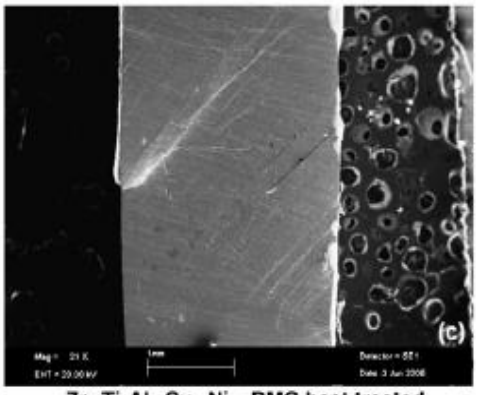

$Zr_{55}Ti_5Al_{10}Cu_{20}Ni_{10}$-BMG heat treated

Following the results obtained at the ESRF, we further examined the role of the presence of such nanocrystals in the ductilisation process as described in our joint publications listed at the end of this report. We have found that they end up growing at crack fronts and forcing cracks to blunt and deviate from the maximum shear plane, thus leading to shear delocalisation (formation of other shear bands), as observed. The SEM images below present this scenario for a crack with intial tip only 10 nm wide (in a).

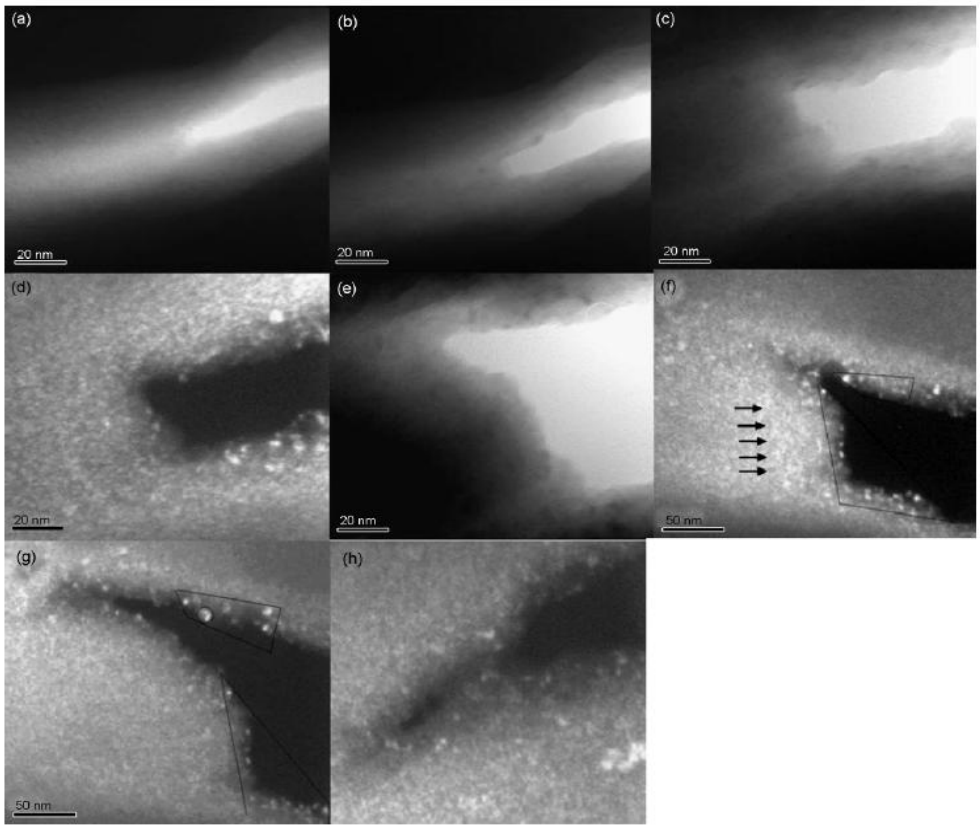

). Blocked crack widening as it tries to escape blockage (a–h). The dark-field image (f) shows clearly how the crack widens facing a zone of nanoparticle clusters

Detection of deviations from ideal solution behavior in Zr-Cu metallic glasses with addition of Al

Using real space pair distribution functions (PDFs) derived from x-ray diffraction data, we probed the atomic level structure of metallic glasses based on Zr and Cu and investigated the effect of a third element (Al) in their atomic structure. The results provide a guide for producing thicker alloy glasses with enhanced functionalities.

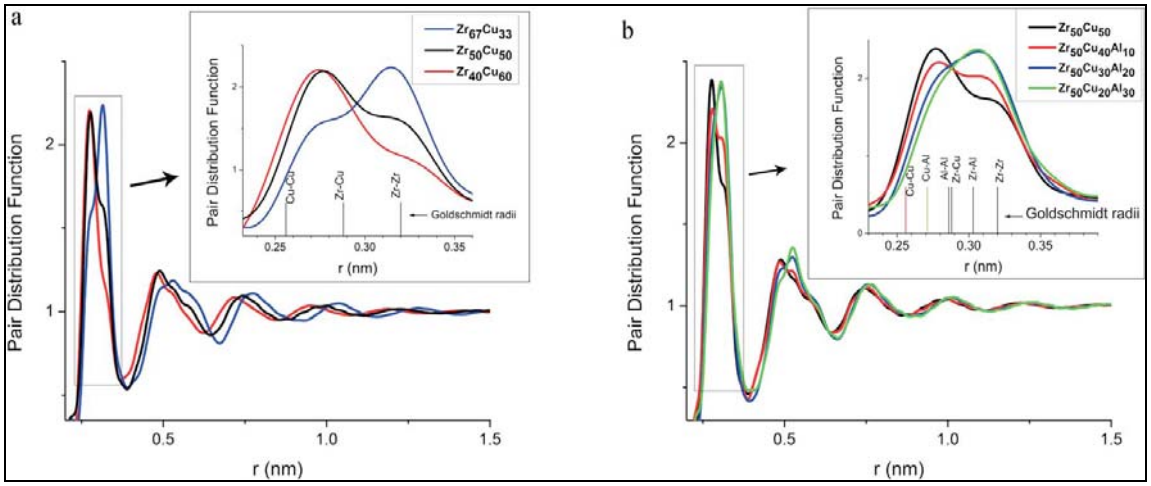

Pair distribution functions for Zr-Cu binary (a) and Zr-Cu-Al ternary (b) metallic glasses. Insets: close-up of the first PDF peak.

The PDFs of the Zr-Cu binary metallic glasses (figure a above) reveal how the atomic structure changes with the Zr/Cu atomic ratio. Increasing Cu content generates significant differences in the PDFs, suggesting modifications in the short (SRO) and medium range order (MRO) up to 1.5 nm. As expected, the structural changes in the nearest neighbor (nn) shell [inset figure a] indicate an increased number of Zr-Zr atomic bonds for the Zr-rich compositions, and increased number of Cu-Zr and Cu-Cu atomic bonds for the Cu-rich site.

Addition of Al to the Zr-Cu metallic glasses leads to significant modifications of short (SRO) and medium range order (MRO), figure b above. The nn shell [inset figure b above] indicates the formation of a significant number of Zr-Al atomic bonds. This behavior can be attributed to strongly attractive Zr-Al atomic interactions consistent with the highly negative heat of mixing ΔH_{mix} of -44 kJ/mol which is twice as negative as for Zr-Cu (-23 kJ/mol) whereas ΔH_{mix} for Cu-Al is negligible (-1 kJ/mol). Al has an intermediate atomic size between those of Zr and Cu atoms. Because of the strongly negative heat of mixing between Zr and Al atoms, addition of Al promotes chemical short range ordering in the liquid, improves the local packing efficiency and slows down long range atomic diffusion required for crystallization, leading to increased glass forming ability (GFA).

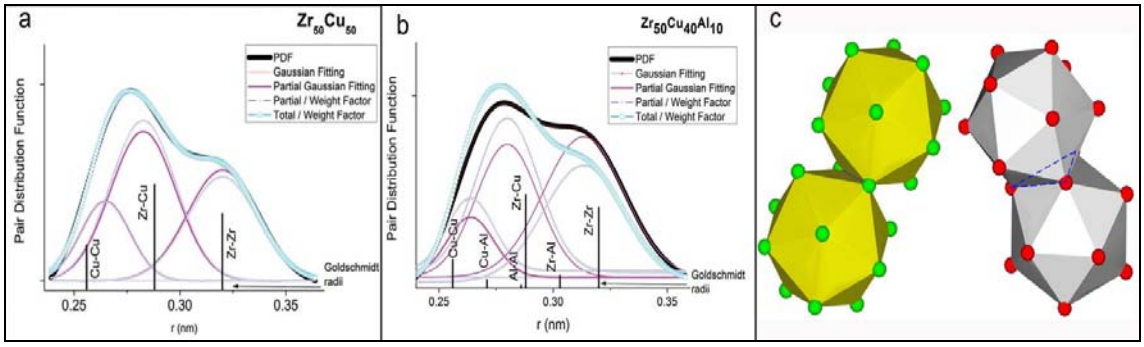

Gaussian fitting of the first PDF peak for a) $Zr_{50}Cu_{50}$ and b) $Zr_{50}Cu_{40}Al_{10}$ metallic glasses. Thick black curves: experimental PDF, thin red curves: calculated partial PDFs derived from the experimental PDF, thin blue discontinuous curves: Gaussian partial PDFs scaled to the weight factors of an ideal solution and thick discontinuous light blue curves: expected total PDFs based on the weight factors, c) schematic diagram showing how the atoms in Zr–Cu based metallic glasses form icosahedral clusters that pack tightly together by sharing faces (right) or edges (left).

For an ideal solution, the total pair distribution function (PDF) for Zr-Cu binary alloys would be correlated with the partial PDF of Zr-Zr, Zr-Cu, and Cu-Cu atomic pairs according to the following relation.

$$G(r)=W_{ZrZr}G_{ZrZr}+W_{CuCu}G_{CuCu}+2W_{ZrCu}G_{ZrCu} \quad (2)$$

Approaching the ternary ZrCuAl alloys as ideal solutions, the correlation between total and partial PDFs would be given as following:

$$G(r)=W_{ZrZr}G_{ZrZr}+W_{CuCu}G_{CuCu}+W_{AlAl}G_{AlAl}+2W_{ZrCu}G_{ZrCu}+2W_{ZrAl}G_{ZrAl}+2W_{CuAl}G_{CuAl} \quad (3)$$

where $W_{ij}= C_iC_jF_iF_j/(\Sigma\ C_iF_i)^2$, W_{ij} are the ideal solution weight factors, C_i are the atomic concentrations and F_i are the atomic form factors .

The PDFs deriving from experimental XRD results for Zr-Cu binary metallic glasses were found to be in good agreement with those expected from the weight factors of equations (2,3) (figure a above), indicating that the Zr–Cu metallic glass can be satisfactorily approximated as an 'ideal solid solution'. Because of the weak interactions between Zr-Cu atoms in the binary alloy, only very thin glasses can be cast from Zr–Cu liquid alloys. However, adding a third strongly interacting component, aluminum (Al), to the liquid alloy leads to a stronger glass that can be cast at thicknesses of up to several millimeters.
We have therefore determined that in contrast to the binary Zr–Cu, ternary Zr–Cu–Al metallic glasses deviate markedly from ideal solution behavior (figure b above). Zr–Cu–Al glasses are comprised of finite regions of atomic order, providing the extra support needed to form thicker glasses. This phenomenon is believed to be due to attractive interactions between the sp-electrons of aluminum and the d-electron shell of the larger zirconium atoms. The atoms arrange in clusters resembling icosahedra, which pack together tightly in the glass (figure c above), as observed in a previous study [Ch.E. Lekka et al, Appl. Phys. Lett. 91 (2007) 214103].

The atomic structure of Zr-Ni and Zr-Ni-Al metallic glasses

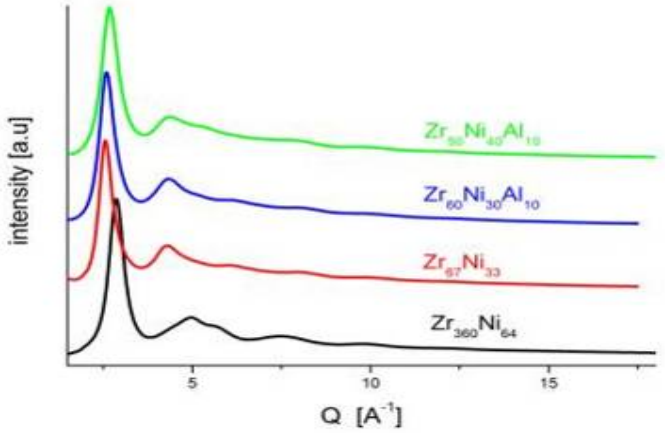

X-ray diffraction patterns of Zr-Ni and Zr-Ni-Al metallic glasses.

The above figure shows the X-ray diffraction patterns of Zr-Ni binary and Zr-Ni-Al ternaries metallic glasses. Successive diffuse haloes can be observed, which are characteristic of amorphous phases. Differences in the features and positions of the diffuse haloes in the Q axis for the various compositions can be noticed implying differences in the atomic structure. However these structural differences become clearer after the Fourier transformation of XRD into real space pair distribution functions PDF.

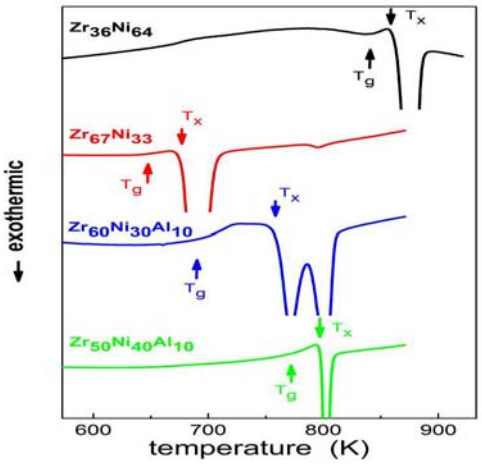

DSC thermograms of Zr-Ni and Zr-Ni-Al metallic glasses.

The glass transition (T_g) and crystallization temperatures (T_x) for these glasses are shown in the above DSC traces. It is interesting to note the increase of the supercooled liquid region $\Delta T_x = T_x - T_g$ from 29 K to 70 K and the crystallization temperature from 676 K to 758 K comparing $Zr_{67}Ni_{33}$ and $Zr_{60}Ni_{30}Al_{10}$, indicating a significant increase of the stability of the supercooled liquid state with the addition of 10% Al in the binary $Zr_{67}Ni_{33}$ metallic glass.

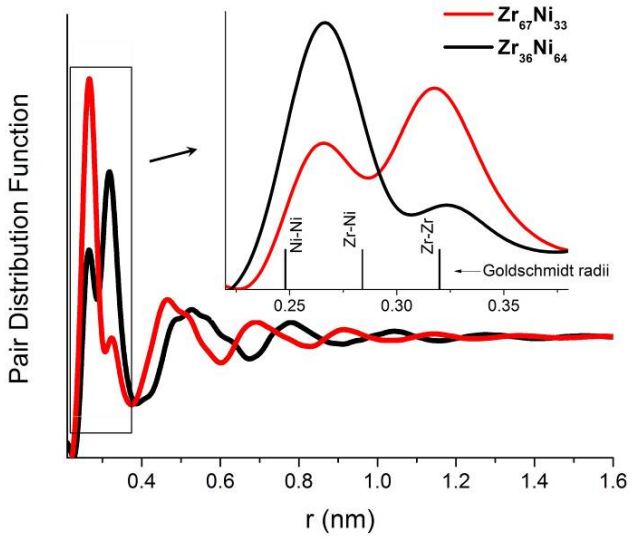

PDFs of Zr–Ni binary metallic glasses (inset: close-up of the nearest neighbor peak).

The above figures shows the calculated atomic pair distribution functions (PDF) of a Zr rich and a Ni rich binary metallic glass. The PDFs reveal short (SRO) and medium (MRO) range ordering up to r=1.5nm. Significant differences in the PDFs can be observed until the fifth peak. The inset shows the structure of the nearest neighbor (NN) shell. The interatomic distances according to the Goldsmidt radii, are also shown. The first PDF peak splits in two maxima. For $Zr_{67}Ni_{33}$, the maximum on the right shoulder is centered around r = 0.318 nm and corresponds to the contribution of Zr-Zr atomic pairs. The maximum on the left shoulder, centered around r = 0.266 nm corresponds mainly to the contribution of Zr-Ni atomic pairs while the contribution of Ni-Ni bonds is expected to be very small.

As expected, in the case of the Ni-rich $Zr_{36}Ni_{64}$, the maximum on the right shoulder, attributed to Zr-Zr atomic pairs, is significantly smaller compared to that of Zr-rich $Zr_{67}Ni_{33}$ whereas the left shoulder attributed to Zr-Ni and Ni-Ni atomic pairs is strongly enhanced. The maximum due to Zr-Zr pairs is centered around r=0.323 nm, while the contribution of Zr-Ni atomic pairs was found to be centered around r=0.271 nm and that of Ni-Ni pairs around r=0.254 nm. A noticeable shrinkage of the average bond length of Zr-Ni atomic pairs in the range of 5-6% compared to the sum of Goldschmidt radii can be seen for the binary Zr-Ni metallic glasses. This shrinkage is due to the strong chemical interaction and electron sharing between Zr and Ni atoms resulting in the large negative enthalpy of mixing between these two elements. On the other hand, the average interatomic distance of similar pairs Zr-Zr and Ni-Ni, is found to be close to the sum of Goldschmidt radii.

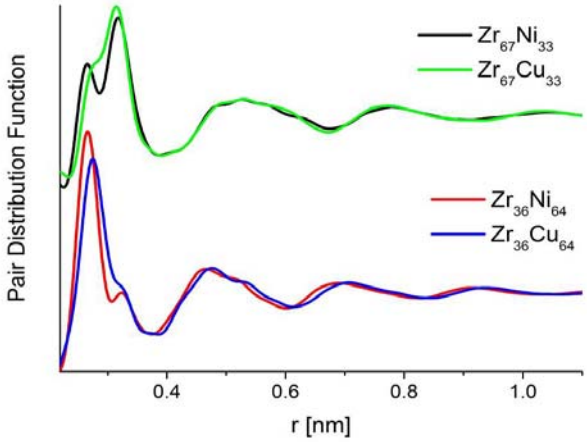

Comparison of PDFs of Zr–Ni and Zr-Cu binary metallic glasses

Because of the similar atomic size of Ni with Cu atoms, it is interesting to compare these PDFs of Zr-Ni to those of Zr-Cu binary metallic glasses. The positions and the main features of the second and higher PDF peaks of $Zr_{67}Ni_{33}$ and $Zr_{67}Cu_{33}$, (figure above), are similar indicating some resemblance in the MRO of the two metallic glasses. However, significant difference can be noticed in the first PDF peak, implying differences in the nearest neighbor shell of the local atomic structure. The strong splitting observed for $Zr_{67}Ni_{33}$, which is associated to the shrinkage of the average bond length of Zr-Ni atomic pairs, is much weaker in $Zr_{67}Cu_{33}$. The left shoulder is slightly shifted at lower distances in the case of $Zr_{67}Ni_{33}$ compared to $Zr_{67}Cu_{33}$, while the right shoulder (attributed to Zr-Zr pairs) is at similar distances for both metallic glasses. It has been suggested, that the dominant structural unit in Zr rich Zr-Ni metallic glasses is a prism type polyhedron, whereas the local atomic structure of Zr–Cu glassy alloys consists of clusters of atoms with mainly icosahedral symmetry.

There are similar differences between the 1st PDF peaks of Zr-poor binary Zr-Ni and Zr-Cu metallic glasses: the split into two maxima is much more pronounced in $Zr_{36}Ni_{64}$ than in $Zr_{36}Cu_{64}$ and the left maximum corresponding to Zr-Ni and Ni-Ni interatomic distances of $Zr_{36}Ni_{64}$ is enhanced compared to $Zr_{36}Cu_{64}$. In addition, the position of the center of gravity of the second and higher order peaks of $Zr_{36}Ni_{64}$ PDF are slightly shifted to lower distances (r) compared to $Zr_{36}Cu_{64}$.

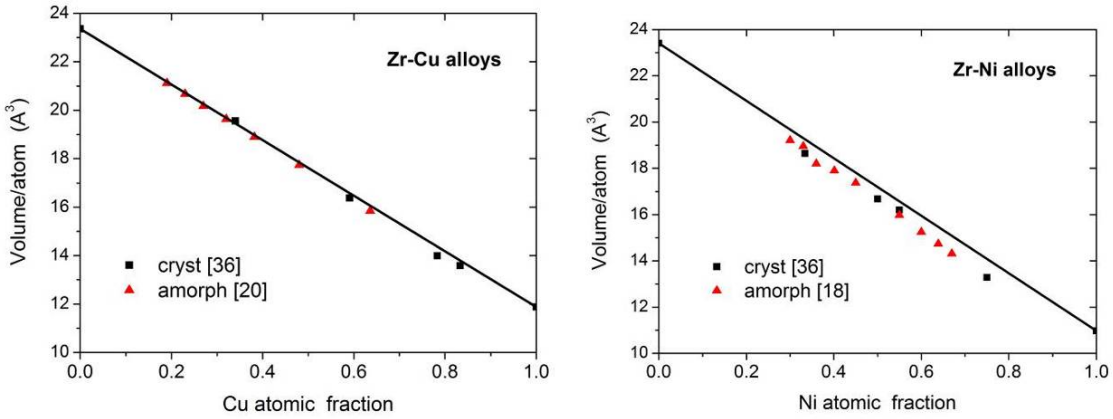

a b

Average atomic volume V as a function of composition for amorphous and crystalline Zr-Cu and Zr-Ni alloys. The solid line corresponds to Vegard's law with zero ΔV_{mix}.

The atomic volumes of Zr-Cu and Zr-Ni binary alloys are shown in the above figure. The solid lines correspond to the empirical Vegard's law linear relation.

The difference between the real atomic volume V_{A-B} and the Vegard's law value (solid lines) at any given composition corresponds to the volume of mixing ΔV_{mix}. The atomic volumes of amorphous and crystalline phases almost coincide, confirming suggestions that the ΔV_{mix} of the crystalline state can be an excellent approximation for the ΔV_{mix} of the glassy state. In addition, for the case of Zr-Cu, it can be seen that the atomic volumes are in good agreement with Vegard's law, implying constant atomic volumes for each constituent (Zr and Cu) over the examined compositional range and indicating an ideal solution behavior for the binary Zr-Cu metallic glasses. As presented earlier in this text, our results at the ESRF show that the ideal solution is a good approximation for the local atomic structure in the Zr–Cu binary glasses. This is due to the fact that Cu atoms have a filled 3d shell and relatively weak interactions with Zr atoms leading to a random atomic arrangement in the Zr-Cu amorphous alloys. Therefore the widely accepted SRO of mainly icosahedral symmetry of Zr-Cu metallic glasses is mainly of topological (TSRO) rather than of chemical (CSRO) origin.

On the other hand, for the case of Zr-Ni small deviations from Vegard's law can be observed (with highest $\Delta V_{mix}/\Delta V_{A-B}$. values of the order of a few percent). Stronger attractive interactions between Ni and Zr are associated with the unfilled d-band of Ni atoms which promotes stronger bonding with Zr atoms via more effective hybridization. The stronger bonds lead to a stronger CSRO and away from the ideal solution behavior.

In order to verify the deviations from the ideal solution behavior implied by the above approach of volumes of mixing, we perform the following analysis of the first peak of the PDFs for two Zr-Ni binary metallic glasses using the well known relation between the total pair distribution function (PDF) and the partial PDF of Zr-Zr, Zr-Ni, and Ni-Ni atomic pairs in Zr-Ni binary glasses:

$G(r)= W_{ZrZr}G_{ZrZr}+ W_{NiNi}G_{NiNi}+ 2W_{ZrNi}G_{ZrNi}$

where $W_{ij}= C_iC_jF_iF_j/(\Sigma\ C_iF_i)^2$, W is the weight factor, C_i is the concentration and F_i is the atomic form factor of the i- atom.

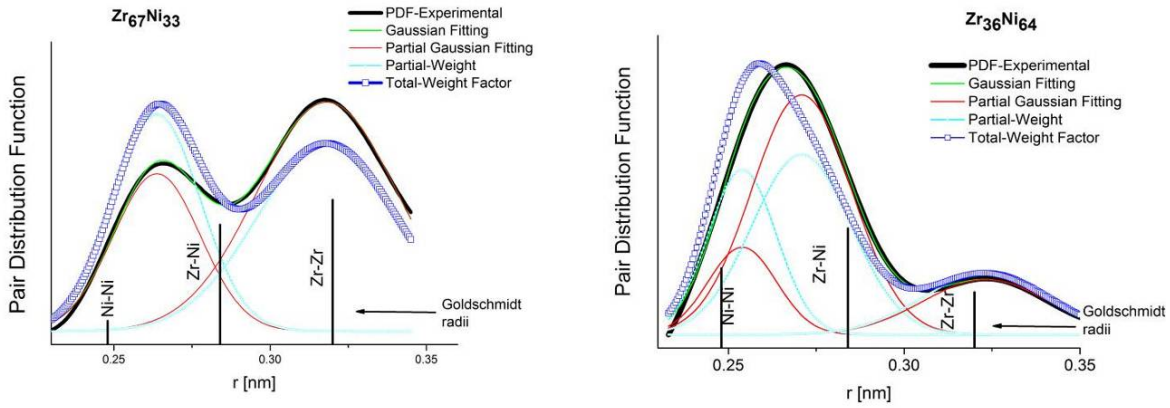

a b

Gaussian fitting of the first PDF peak of a) $Zr_{67}Ni_{33}$ and b) $Zr_{36}Ni_{64}$ metallic glasses. The thick continuous black curves correspond to the experimental PDF, the thin red continuous curves correspond to partial PDFs derived from the deconvolution of the experimental PDF. The thin blue discontinuous curves represent the Gaussian partial PDFs if they are scaled to the weight factors of an ideal solution and the thick discontinuous blue curves represent the expected total PDFs based on the weight factors.

A satisfactory fitting of the first PDF peak for $Zr_{67}Ni_{33}$ can be obtained using two Gaussian peaks corresponding to Zr-Zr and Zr-Ni, interatomic distances (thin continuous red curves),. The contribution of Ni-Ni pairs is expected to be small. Contrary to the case of Zr-Cu metallic glasses, the relative area below the three partial Gaussian peaks cannot be scaled with the ideal solution weight factors and the expected PDFs based on weight factors (thick blue curves) deviates significantly from the experimental PDF (black curve). Similarly, the relative area below the three convoluting peaks for $Zr_{36}Ni_{64}$ are observed to deviate from the expected behaviour based on the weight factors. The analysis indicates strong deviations from the ideal solution model because of the strong chemical interaction between Zr and Ni atoms, confirming the above observations from the volumes of mixing approach.

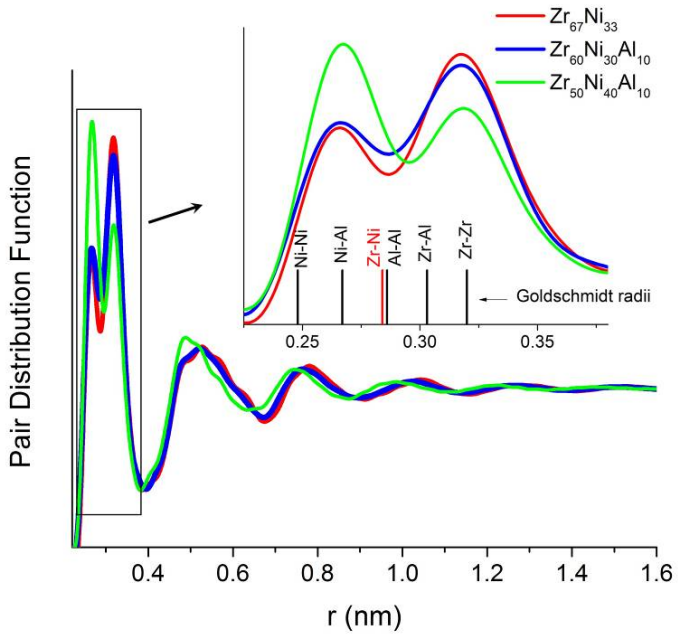

PDFs of Zr–Ni-Al ternary glasses (inset: close-up of the nearest neighbor peak).

Above we present PDFs of ternary Zr-Ni-Al metallic glasses in comparison with that of binary $Zr_{67}Ni_{33}$. Addition of 10at.% Al in $Zr_{67}Ni_{33}$ ($Zr_{60}Ni_{30}Al_{10}$) modifies slightly the PDF. Similarly to the case of $Zr_{67}Ni_{33}$, the nearest neighbor peak of $Zr_{60}Ni_{30}Al_{10}$ consists of two maxima, one at low r (r≈0.266 nm) and another at higher r (r≈0.318 nm) with a clear split between the two maxima. The differences can be mainly attributed to a small decrease in the number of Zr-Zr atomic pairs and the appearance of Ni-Al and Zr-Al atomic pairs in the nearest neighbor (NN) shell of $Zr_{60}Ni_{30}Al_{10}$. A comparison of the PDF of $Zr_{50}Ni_{40}Al_{10}$ with that of $Zr_{60}Ni_{30}Al_{10}$, indicates less Zr-Zr pairs and a strong increase in the number of Zr-Ni pairs in the NN shell of $Zr_{50}Ni_{40}Al_{10}$

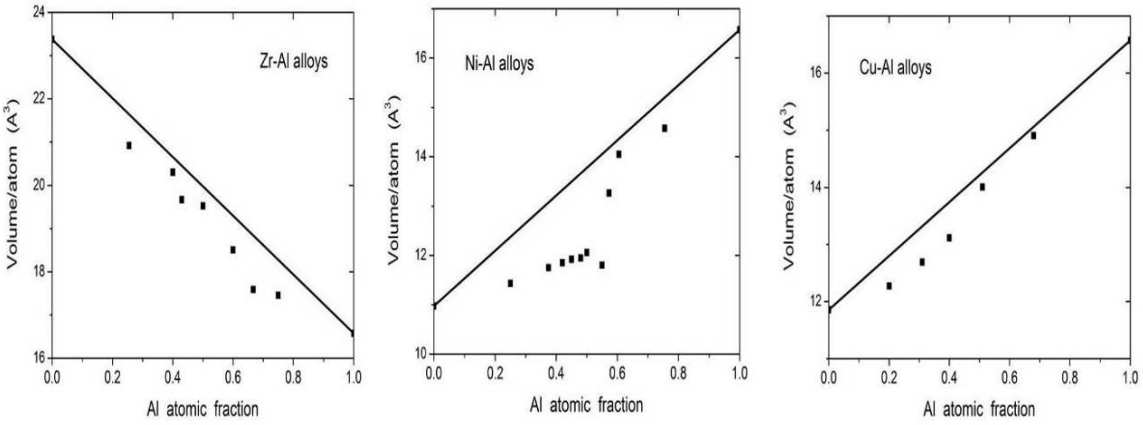

Average atomic volume V as a function of composition Zr-Al, Ni-Al and Cu-Al alloys. The solid line corresponds to Vegard's law with zero ΔV_{mix}.

The above figure shows the volumes per atom of Zr-Al, Ni-Al and Cu-Al binary alloys. Contrary to the case of Zr-Ni and Zr-Cu discussed earlier, the atomic volumes in all three Al containing binary systems show strongly negative ΔV_{mix}. Addition of Al in Zr-Ni or Zr-Cu metallic glasses can thus strongly reduce atomic volumes leading to structures with higher packing density. Al has an intermediate atomic size (0.143 nm) between those of Zr (0.160 nm) and Ni (0.124 nm) atoms. Indeed as shown in the DSC traces presented earlier, addition of Al to $Zr_{67}Ni_{33}$ improves noticeably the stability of the supercooled liquid state by increasing the crystallization temperature (T_x) from 676K to 758K and the supercooled liquid region ($\Delta T_x = T_x - T_g$) from 29K to70K.

For the case of Zr-Cu metallic glasses it was shown that Al addition promotes strong deviations from the ideal solution behavior. For the case of Zr-Ni, Al addition is expected to induce further deviations from ideal solution behavior, which are already present in the binary alloy.

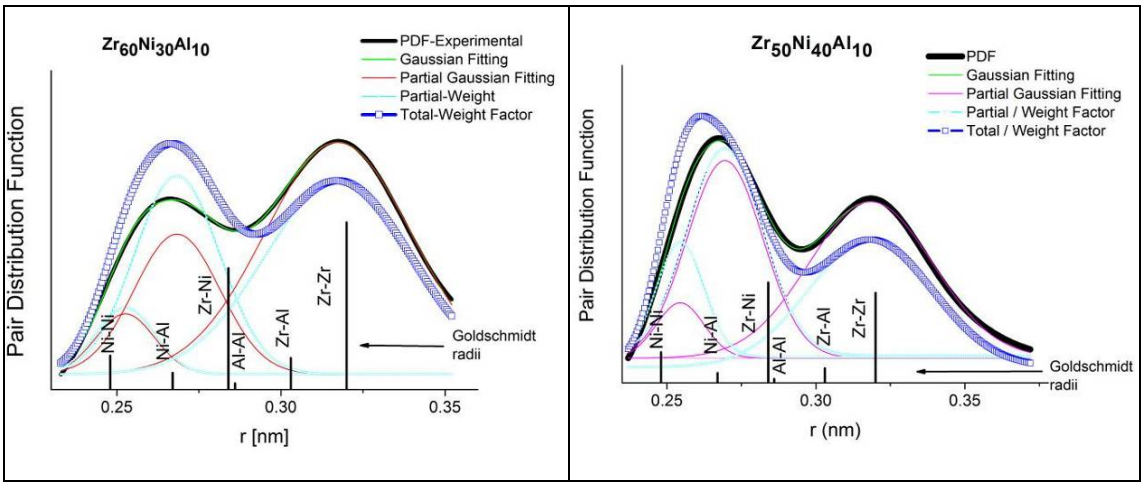

Gaussian fitting of the nearest neighbor peak of a) $Zr_{60}Ni_{30}Al_{10}$ and b) $Zr_{50}Ni_{40}Al_{10}$ metallic glasses. The thick continuous black curves correspond to the experimental PDF, the thin red continuous curves correspond to partial PDFs derived from the deconvolution of the experimental PDF. The thin blue discontinuous curves represent the Gaussian partial PDFs if they are scaled to the weight factors of an ideal solution and the thick discontinuous blue curves represent the expected total PDFs based on the weight factors.

We used the following relation between total and partial PDFs.

$$G(r)= W_{ZrZr}G_{ZrZr}+ W_{NiNi}G_{NiNi}+ W_{AlAl}G_{AlAl}+ 2W_{ZrNi}G_{ZrNi}+ 2W_{ZrAl}G_{ZrAl}+ 2W_{NiAl}G_{NiAl} \quad (3)$$

where $W_{ij}= C_iC_jF_iF_j/(\Sigma\ C_iF_i)^2$, W_{ij} are the ideal solution weight factors, C_i are the atomic concentrations and F_i are the atomic form factors .

A satisfactory Gaussian fitting of the nearest neighbor peak of the Zr-Ni-Al ternary metallic glasses can be obtained using 3 peaks (continuous red curves). We assume the three partial peaks to be convolutions of the contributions of nearby peaks due to Ni-Ni and Ni-Al (first Gaussian), Zr-Ni and Al-Al (second Gaussian), and Zr-Al and Zr-Zr (third Gaussian) atomic pairs respectively, bearing in mind that the contribution of Al-Al and Ni-Al pairs is expected to be small. We apply the approach of three convoluting peaks instead of six, in order to simplify the fitting process, since fitting with six peaks would give less reliable results. As expected, comparing the relative areas below these peaks, it can be observed that they cannot reproduce the experimental total PDF when scaled to the ideal solution weight factors. The solid solution approach does not take into account chemical interactions between the atoms, and is based only on nearest neighbor probability distributions that scale with the compositions and the X-rays diffraction atomic form factors.

Remarks concerning, Time Table and Milestones:

The implementation of this research was somewhat slowed by the construction work for the creation of the new X-ray microscope on the ID11 beam line facilities "Nanoscope". As such, our project implementation occurred over more than 4 years instead of the initially planned 3 years.

Additional benefits from the Nanoscope on ID-11

Our project benefited from the availability of this X-ray microscope configuration and μm or submicron size beam on ID11 and we give two examples here.

The first example is the investigation of structure gradients in a Cu-rich "chill-zone" CuZr-type alloy too rich in Cu to be glassy. The gradual transition from a 2 nm-scale nanostructure on the surface to relatively coarse microstructure 100 μm into the sample can be seen in the next image and was presented in Acta Mater in a joint publication in 2008.

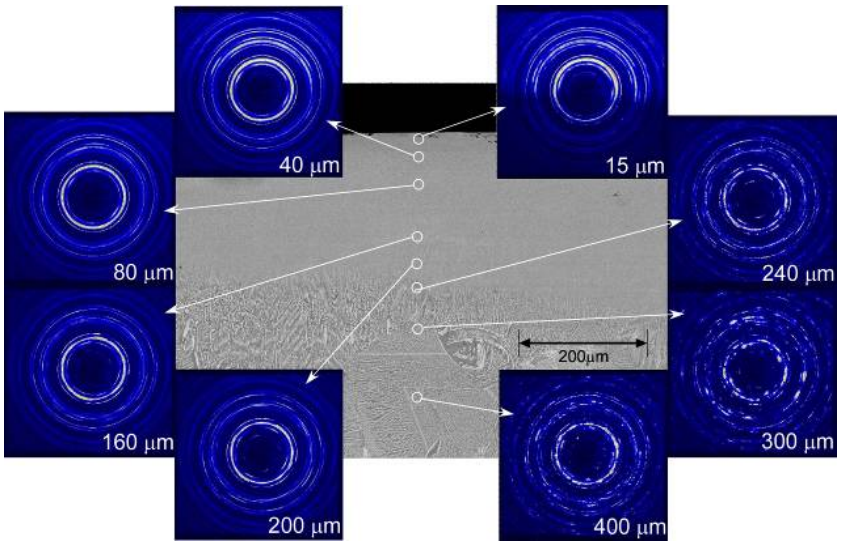

The second example (as yet unpublished) is for a Pd-based metallic glass tape that was bent and XRD micro-profiling was performed on the bend in transmission using a submicron beam size. As seen in the next image and the accompanying diffraction patterns, nanocrystallisation was detected on the compression side but not on the tension side of the neutral fibre axis. This would have been impossible without a very small focused beam of high brilliance.

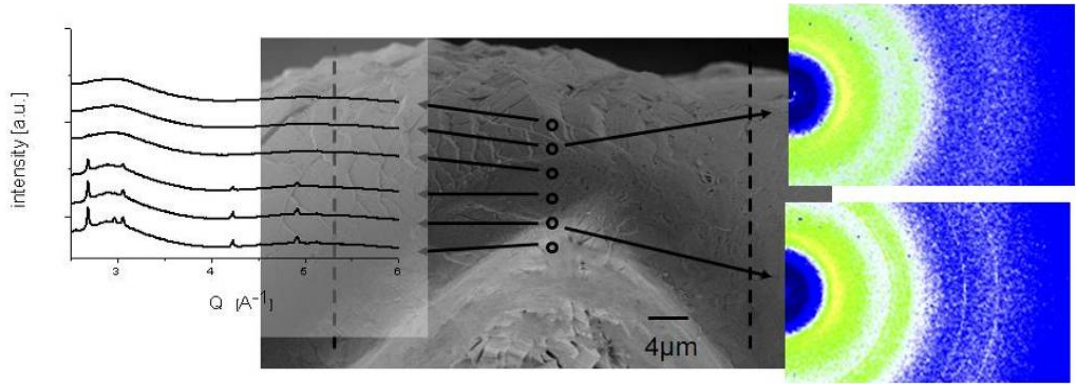

Time Table and Milestones:

Dr Magnus Bostrom was employed as postdoc at the ESRF and served in support of this project for 24 months (2005-2006). He was supported by the European RTN Network MRTN-CT-2003-504692 associated to this project. Many other students and postdocs supported by the EC also participated in the research and training activities at the ESRF.

Milestone I:
Confirmation of generalization or limitation of use of eq. (1) for metallic glasses as compared to oxide glasses was achieved by comparison of temperature shifts of real space (pdf) and reciprocal (diffraction) data.

Milestone II:
Establishment of structural changes and excess free volume in glasses quenched from liquid state was achieved

Milestone III:
Establishment of structural changes and free volume generation during deformation to various plastic strains was achieved.

Milestone IV:
Comparison of measured values of activation energy for free-volume relaxation using our method and results with those of the literature obtained by methods other than XRD was achieved.

ME-1163 (LT) led to to many other achievements not initially expected. For the ensemble of the achievements, the ESRF evaluation is referred to our long list of joint publications below

Developments expected to be of benefit to other users:

We had previously purchased for about 20,000 euros, a protable high frequency generator for in-the-beam induction heating. This useful portable generator is freely available for use by other ESRF users. We have also recently purchased (8000 euros), a new high-T vacuum-tight Linkam hotstage that is also available to other users.

The XRD method for free-volume and relaxation measurements that we have devised is useful for others and in particular is now being used by researchers at synchrotrons in the USA and in Japan (who cite our work at the ESRF).

ACKNOWLEDGEMENTS: ***We are grateful to the ESRF for having been a major partners for us in the past decades. We wish to express our deep gratitude to the ID-11 and ID-15 beam-lines staff for their efficient, competent and kind support during our experiments. We are particularly and continuously impressed and inspired by the scientific competence and expertise, hard work and exceptional human qualities of the ID-11 Chief Scientist Dr Gavin Vaughan***

ESRF Publications Long Term Project ME-1163

1. "Glass Transition Tg and Thermal Expansion in Glassy Materials Measured by Time-Resolved X ray Diffraction" K Ota, K hajlaoui, G Vaughan, M.Di Michiel, D.V. Louzguine, A. Inoue, A.R Yavari, *Journal of Metastable and Nanocrystalline Materials,* Vol. 24-25 (2005) pp. 225-228.

2. "X-ray Diffraction Studies of Thermal Expansion, Free Volume Change and Glass Transition Phenomenon in Cu-based Glassy and Nanocomposite Alloys on Heating", D.V. Louzguine, A.R.Yavari, K. Ota, G. Vaughan, A. Inoue, *Journal of Non-Crystalline Solids*, 351 (2005), pp. 1639-1645.

3. "Glass Transition T_g, Thermal Expansion, and Quenched-in Free Volume ΔV_f in Pyrex Glass Measured by Time-Resolved X-ray Diffraction", K.Ota, W.J.Botta, G.Vaughan , A.R.Yavari, *Journal of Alloys and Compounds*, 388 (2005) L1–L3.

4. "Transition Metal and Transition Metal Fluorides as Catalysts in MgH_2-based Nanocomposites" W.J.Botta F., J.F.R. de Castro, G. Vaughan , A.R. Yavari, *Journal of Metastable and Nanocrystalline Materials*, 24-25 (2005) pp. 299-304.

5. "Excess free volume in metallic glasses measured by X-ray diffraction", A.R.Yavari, A. Le Moulec, A. Inoue, N. Nishiyama, N. Lupo, E. Matsubara, W.J.Botta F., G. Vaughan, M. di Michiel , A. Kvick, *Acta Materialia*, 53 (2005) pp. 1611-1619.

6. "Shear delocalisation and crack blunting of a metallic glass containing nanoparticles: in-situ TEM" K. Hajlaoui, A.R. Yavari, B. Doisneau, A. LeMoulec, G. Vaughan, A.L. Greer, A. Inoue, A. Kvick, *Scripta Materialia* 54 (2006) pp. 1829-1834

7. "Unusual room temperature ductility of glassy Cu-Zr caused by nanoparticle dispersions that grow during shear" K. Hajlaoui, B. Doisneau, A.R. Yavari, W. Zhang, G. Vaughan, A. Inoue and A.L. Greer *Mater Sci and Eng A* 449-451 (2007) 105-110

8. "Thermal expansion of a glassy alloy studied using real-space pair distribution function", D. Louzguine, A. Inoue, A.R. Yavari, G. Vaughan, *Appl. Phys. Lett*., 88 (2006) 121926-8

9. "X-ray Diffraction in Materials Science: Excess Free Volume ΔVf in Metallic Glasses Measured by X-ray Diffraction" A.R. Yavari, *ESRF Highlights* 2005, pp.35-36

10. "Free Volume Change upon Structure Relaxation and Devitrification Behavior of Hf-Pd-Ni Glassy Alloy on Heating", D.V. Louzguine, L.V. Louzguina, A.R. Yavari, K. Ota, G. Vaughan, A. Inoue, *Thin solid films*, 609 (2006) 75-80

11. "Free volume and elastic property changes in Cu-Zr-Ti-Pd bulk glassy alloy on heating" D. Louzguine, A.R. Yavari, K. Ota, G. Xie, G. Vaughan, A. Inoue *J. Alloys and Compounds* 431 (2007) 136-140

12. F.O. Méar, F.G. Vaughan, A.R. Yavari and A.L. Greer, Residual-stress distribution in shot-peened metallic-glass plate, *Phil. Mag. Lett.* 88 (2008) 757-766

13. "Ductilization of BMGs by optimization of nanoparticle dispersion" K. Hajlaoui, A.R. Yavari, J. Das, G. Vaughan, *J. Alloys and Compounds*, 434-435 (2007) 6-9

14. "Plasticity induced by nanoparticle dispersions in bulk metallic glasses" K. Hajlaoui, A.R. Yavari, A. LeMoulec, W.J. Botta, G. Vaughan, J. Das, A.L. Greer, A. Kvick, *J. Non-Cryst. Solids* 353 (2007) 327-331.

15. Cu Rich Nanostructured Alloys with Enhanced Mechanical Properties, K. Georgarakis, K. Ota, A. LeMoulec, F. Charlot, A. R. Yavari and G. Vaughan, Materials Research Society -2007 Fall Meeting, Symposium HH: Nanophase and Nanocomposite Materials V, Mater. Res. Soc. Symp. Proc. 1056-HH08-52.

16. "Plasticity in bulk metallic glasses investigated via the strain distribution", J. Das, M. Boström, A. Kvick, A.R. Yavari, A.L. Greer, J. Eckert, *Physical Review B* 76 (2007) 092203-092207

17. Free volume and elastic properties changes in Cu–Zr–Ti–Pd bulk glassy alloy on heating, D.V. Louzguine-Luzgin, A.R. Yavari, M. Fukuhara, K. Ota, G. Xie, G. Vaughan, and A. Inoue, *J. Alloys Compounds*. 431, 136 (2007).

18. Chill zone copper with the strength of stainless steel and tailorable color, A.R. Yavari, K. Ota, K. Georgarakis, A. LeMoulec, F. Charlot, G. Vaughan, A.L. Greer and A. Inoue, *Acta Materialia*, 56
19. (2008) 1830-1839

20. Real-space structural studies of Cu–Zr–Ti glassy alloy, D. V. Louzguine, J. Antonowicz, K. Georgarakis, G. Vaughan, A. R. Yavari, A. Inoue, *Journal of Alloys and Compounds*, *Volume 466, Issues 1-2*, *20 October 2008*, *Pages 106-110*

*21. "*Glass transition, thermal expansion and relaxation in B2O3 glass measured by time-resolved X, ray diffraction", W.J. Botta, K. Ota, K. Hajlaoui, G. Vaughan, A.R. Yavari, *Journal of Non-Crystalline Solids* 354 (2008) 325–327.

22. "Residual-stress distribution in shot-peened metallic-glass plate", F.O. Mear, G. Vaughan, A.R. Yavari and A.L. Greer, *Phil. Mag. Lett.* 88 (2008) 757-766

23. "In-situ X-ray diffraction of mechanically milled beta-Al3Mg2 powders", Scudino S., Sakaliyska M., Stoica M., Surreddi K.B., Ali F., Vaughan G., Yavari A.R., Eckert J., Physica Status Solidi-Rapid Research Lett. 2 (2008) 272

24. Crystallization kinetics and magnetic properties of $Fe_{66}Nb_4B_{30}$ bulk metallic glass, M. Stoica, S. Kumar, S. Roth, S. Ram, J. Eckert, G. Vaughan, A.R. Yavari, *Journal of Alloys and Compounds*, 483 (2009) 632-637

25. *"*Atomic structure of Zr-Cu-Al and Zr-Ni-Al amorphous alloys", J. Antonowicz , D.V. Louzguine-Luzgin, A.R. Yavari, K. Georgarakis, M. Stoica, G. Vaughan, E Matsubara , A. Inoue, *Journal of Alloys and Compounds*, *471 (2009*) *70-73*

26. Real time synchrotron radiation studies on metallic glass (Zr0.55Al0.1Ni0.05Cu0.3)(99)Y-1 after cold rolling" , Li Y., Georgarakis K., Pang S., Ma C., Vaughan G,, Yavari A.R. , Zhang T., *Intermetallics* 17 (2009) 231-234

27. Clustered crystalline structures as glassy phase approximants, D. V. Louzguine, A. R. Yavari b, G. Vaughan, A. Inoue, Intermetallics 17 (2009) 477–480

28. "Influence of fluxing in the preparation of bulk Fe-based glassy alloys", C. Duhamel, K. G. Georgarakis, A. LeMoulec, A.R. Yavari, G. Vaughan, A. Baron, N. Lupu , *Journal of Alloys and Compounds* 483 (2009) 243–246

29. "Effect of Ag addition on local structure of Cu–Zr glassy alloy", D.V. Louzguine, K. Georgarakis,
30. A. R. Yavari, G. Vaughan, G. Xie, A. Inoue, *J. Mater. Res*., Vol. 24 (2009) 274-278

31. “Atomic structure of Zr–Cu glassy alloys and detection of deviations from ideal solution behavior with Al addition by x-ray diffraction using synchrotron light in transmission”, K. Georgarakis, A. R. Yavari, D. V. Louzguine, J. Antonowicz, M. Stoica,Y. Li, M. Satta, A. LeMoulec, G. Vaughan, and A. Inoue *Applied Phys. Lett.* 94 (2009) 191912